

Proceedings Article

# Helical scanning 3D magnetic particle imaging technology

Ning He<sup>a,b,c</sup>. JiaWei Hu<sup>a,b,c</sup>. Zhonghao Zhang<sup>a,b,c</sup>. Chenxiao Xu<sup>a,b,c</sup>. Pengyue Guo<sup>a,b,c</sup>.  
Yunpeng Gao<sup>a,b,c</sup>. Dawei Ge<sup>a,b,c</sup>. Lei Li<sup>a,b,c</sup>. Qibin Wang<sup>a,b,c</sup>. Yidong Liao<sup>a,b,c</sup>.  
Lingwen Hou<sup>a,b,c</sup>. Kai Liu<sup>a,b,c</sup>. Chenglong Shi<sup>a,b,c</sup>. Man Luo<sup>a,b,c</sup>. Yu Zeng<sup>a,b,c</sup>.  
Yihan Wang<sup>a,b,c</sup>. Shouping Zhu<sup>a,b,c,\*</sup>

<sup>a</sup>School of Life Science and Technology, Xidian University Engineering Research Center of Molecular and Neuro Imaging, Ministry of Education, Xi'an, Shaanxi 710126, China

<sup>b</sup>Xi'an Key Laboratory of Intelligent Sensing and Regulation of trans-Scale Life Information International Joint Research Center for Advanced Medical Imaging and Intelligent Diagnosis and Treatment, School of Life Science and Technology, Xidian University, Xi'an, Shaanxi 710126, China

<sup>c</sup>Innovation Center for Advanced Medical Imaging and Intelligent Medicine, Guangzhou Institute of Technology, Xidian University, Guangzhou, Guangdong 51055, China

\*Corresponding author, email: [spzhu@xidian.edu.cn](mailto:spzhu@xidian.edu.cn)

© 2024 He *et al.*; licensee Infinite Science Publishing GmbH

This is an Open Access article distributed under the terms of the Creative Commons Attribution License (<http://creativecommons.org/licenses/by/4.0>), which permits unrestricted use, distribution, and reproduction in any medium, provided the original work is properly cited.

## Abstract

Magnetic particle imaging (MPI) is a novel emerging tomographic technique with high resolution and high sensitivity. Typically, the magnetic fields of MPI scanners are generated by current-carrying coils, resulting in an immense power consumption and making it difficult to apply in clinical research. Halbach array-based MPI devices offer a new solution that greatly reduces device power consumption while providing high gradients. In this work, a mechanically-driven scanning MPI technique was designed using Halbach arrays. This design enables the device to achieve an imaging field of view (FOV) with a diameter of 45 mm, a simulated imaging resolution better than 0.5 mm, and a power consumption of less than 1.5 kW. The feasibility of the device was analyzed through simulation and image reconstruction. In this design, we used extended PSF and extended FOV after deconvolution reconstruction method, which improves the reconstruction resolution by 2-3 times.

## I. Introduction

Magnetic particle imaging (MPI) is an emerging medical imaging technique to image the distribution of superparamagnetic iron oxide nanoparticles (SPIO). Since its introduction in 2005, MPI has been widely used in bioimaging[1]. However, the immense power consumption limits its upgrade to preclinical applications[2]. We propose a permanent magnet configuration that generates a high-gradient selective field that allows for high-resolution imaging. The device is mechanically driven

for FOV scanning, resulting in lower power consumption compared to a carrier coil device with the same imaging FOV. Moreover, this device can extend the imaging FOV by replacing the Halbach array with a larger diameter.

## II. Method and materials

Power consumption is a critical limiting factor for MPI when it comes to imaging human-sized objects with high resolution. In this design, a new scanning method based

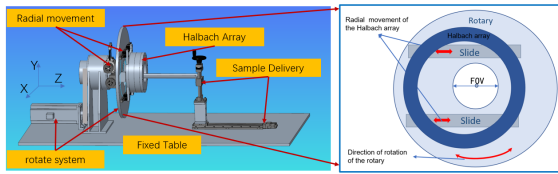


Figure 1: System Architecture

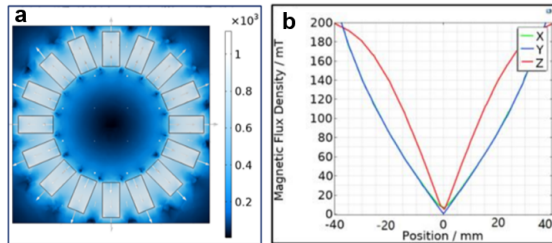


Figure 2: Gradient field simulation. (a) Selected field strength distribution (b) Selected field strength linear distribution with a linear region between -35 mm and 35 mm and an average magnetic field gradient value of 3 T/m.

on the Halbach array is proposed to enhance imaging resolution and reduce power consumption. Based on the scanning method, a helical scanning MPI device was designed as shown in figure 1. The scanning system of the device consists of five main modules: rotation module, radial movement module, Halbach array, sample delivery module, and fixed structure. The rotation module drives the fixed Halbach array on the rotary shaft to rotate, while the radial movement module drives the Halbach array to move radially along the turntable. These two driving modules work in coordination to complete the scanning of the 2D plane. Additionally, axial scanning is employed for achieving 3D scanning and sample delivery. This scanning method allows for multiple scanning trajectories.

### II.I. Selective Field

Figure 2 shows the selection field. We used one layer of nested  $k=0$  Halbach array to generate a field-free point (FFP). The device scans the imaging FOV by mechanically moving the FFP. The simulation results of the selective field are shown in figure 2. The magnetic field gradient value of 3T/m enables a resolution better than 1mm.

### II.II. Scanning Trajectory

The scanning of the device mainly consists of a rotating module and a radial moving module. The rotating module

drives the Halbach array to move in a circular motion with an angular velocity  $\omega$ , and the radial moving module drives the Halbach array to move horizontally with

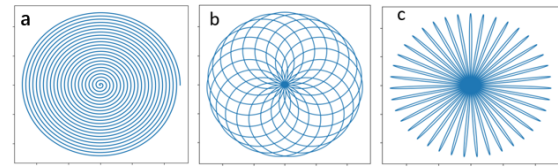


Figure 3: Scanning trajectories. a. Spiral scanning trajectory; b. Flower scanning trajectory; c. Radial scanning trajectory

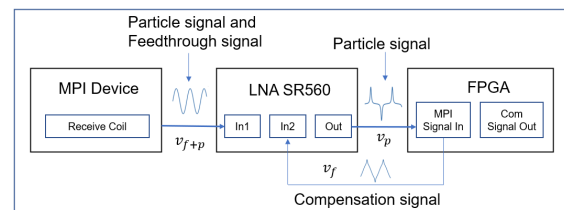


Figure 4: Excitation receiving system. The differential function of LNA SR560 is used to offset the feedthrough signal to obtain the particle signal.

a velocity  $v$ . This ensures that the FFP covers the entire imaging FOV. The position of the FFP is expressed in a Cartesian coordinate system as shown in (1) and (2);

$$\theta = \omega \cdot t, r = v \cdot t \quad (1)$$

$$x = r \cdot \cos\theta, y = r \cdot \sin\theta \quad (2)$$

Where  $v$  [mm/s] is the velocity of radial movement,  $\omega$  [rad/s] is the angular velocity of rotation,  $r$  [mm] is the radial movement,  $\theta$  [rad] is the angular of rotation,  $x, y$  [mm] is the cartesian plane coordinate values. Setting different rotational angular speeds and horizontal movement speeds[3], the following scanning trajectories can be realized, as shown in figure 3.

### II.III. Excitation receiving system

The excitation system of the device uses a sinusoidal excitation current of 25kHz@18A. The receiver module uses a two-stage receiver-compensation coil to receive the nonlinear response signal of the magnetic particles, and uses a low-noise amplifier SR560 for signal filtering and amplification in the receiver link, and fast active compensation based on an FPGA to improve the signal-to-noise ratio by canceling the interference of multiple harmonics, and finally uses a 4MHz acquisition rate for signal acquisition.

### II.IV. Optimal design

The scanning system of the device is performed by a motor driving a Halbach array. The motor generates electromagnetic interference signals during operation, which can affect the MPI magnetic particle nonlinear response

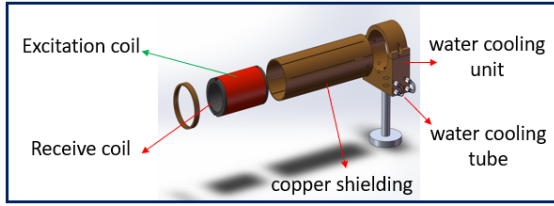


**Figure 5:** Optimized design. The optimized design of the excitation receiving system includes electromagnetic interference shielding design and temperature suppression design.

signal. Therefore, shielding measures for electromagnetic interference in this device are required. The interference frequency of the motor in this device is from 100 Hz to 100 MHz, while the bandwidth of the magnetic particle response signal is from 25 kHz to 2 MHz. According to the skin effect of electromagnetic wave, we use 2 mm copper shielding cover on the motor to shield the motor EMI, and 2 mm copper shielding tube to isolate the excitation receiving system to counteract the external EMI more effectively.

## II.V. Reconstruction method

In this device, we use extended point diffusion and extended imaging field of view for the iterative deconvolution method for reconstruction. Typically, the deconvolution algorithm in the MPI system assumes that the PSF (the derivative of the Langevin function) has a spatial shift-invariance, however, in the realistic system, the PSF changes in the field of view with the FFP scanning, so the use of the PSF causes artifacts and affects the reconstruction resolution. Therefore, in this paper, the extended PSF and extended imaging FOV methods are used for reconstruction, and the extended system realizes the spatial shift-invariance, solves the artifact problem, and improves the reconstruction resolution at the same time. The magnetic particle nonlinear response signal is represented as in (3):

$$u^p(t) = -\mu_0 p^R(H^e)'(t) \cdot c(x) * PSF(x) \quad (3)$$

X-space reconstruction image[4]:

$$Img = -\frac{u^p(t)}{\mu_0 p^R(H^e)'(t)} = c(x) * PSF(x) \quad (4)$$

Based on the X-space reconstruction results,  $Img$  is extended using the method shown in (5), and the extended  $PSF_{ext}$  is obtained using biased MPS measurements. Finally the  $Img_{ext}$  and measured  $PSF_{ext}$  are reconstructed using Lucy-Richardson(LR) deconvolution[5], as shown in (6). The method achieves a resolution better than 0.5 mm under simulation.

$$\widehat{Img_{ext}} = (PSF_{ext} * Img) + Img_{ext} \quad (5)$$

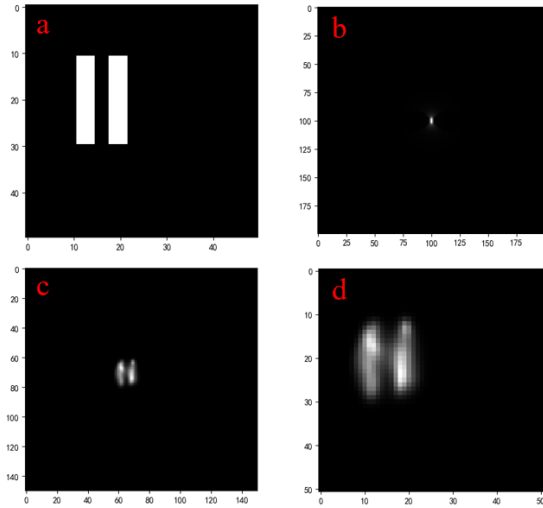


**Figure 6:** Reconstruction method; a) denotes two phantoms with a distance of 2mm, b) denotes the extended PSF, c) denotes the extended FOV, d) denotes the final reconstruction.

$$C_{LR}^{n+1} = C_{LR}^n \left( PSF_{ext} \cdot \frac{\widehat{Img_{ext}}}{C_{LR}^n * PSF_{ext}} \right) \quad (6)$$

Where  $\widehat{Img_{ext}}$  denotes the extended  $Img$  as shown in (5),  $C_{LR}$  denotes the particle concentration obtained by LR deconvolution.

## III. Results

The current design can realize an imaging FOV with a diameter of 45 mm. The simulation results indicate that the imaging resolution of the device is 0.5mm when using 20nm diameter single-core magnetic particles in adiabatic conditions, as shown in figure 7. Additionally, the total power consumption of the device is less than 1.5 kW. Moreover, this device can extend the imaging FOV by replacing the Halbach array with a larger diameter while keeping the total power consumption unchanged.

## IV. Conclusions

The advantages of technology are as follows. This technology structure is simple and reduced power consumption. This technology can enhance the imaging field of view of the device by increasing the diameter of the Halbach arrays. This technology can flexibly increase the size of the permanent magnets to enhance the value of the selected field gradient, thus increasing the imaging resolution of the device. Based on this device, high-resolution 3D imaging can be achieved. In future work, we will use the device for small animal tumor imaging.

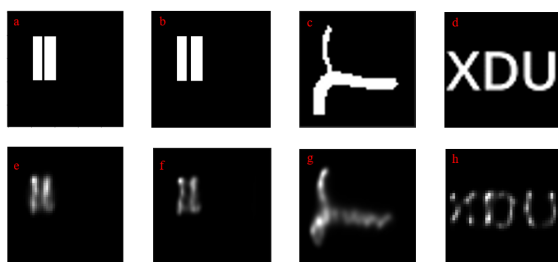


**Figure 7:** Analysis of the simulation reconstruction results. a) denotes two phantoms with a distance of 0.5mm, b) denotes two phantoms with a distance of 1.5mm, c) denotes the blood vessel phantom, d) denotes the letter phantom, e) denotes the 0.5mm phantoms' reconstruction image used extended deconvolution method, f) denotes the 1.5mm phantoms' reconstruction image used extended deconvolution method, g) denotes the blood vessel's reconstruction image e used extended deconvolution method, h) denotes the letter phantom's reconstruction image e used extended deconvolution method.

## Acknowledgments

This work was supported by the National Natural Science Foundation of China under Grant Nos. 62027901, 62071362, 82272050, 61901342, the Natural Science Basic Research Program of Shaanxi Province under Grant Nos. 2021JZ-29, 2021SF-131, 2021SF-169, and the Fundamental Research Funds for the Central Universities under Grant No. JB211205.

## Author's statement

**Conflict of interest:** Authors state no conflict of interest.  
**Informed consent:** Informed consent has been obtained from all individuals included in this study.  
**Ethical approval:** The research related to human use complies with all the relevant national regulations, institutional policies and was performed in accordance with the tenets of the Helsinki Declaration, and has been approved by the authors' institutional review board or equivalent committee.

## References

- [1] Gleich, B. and J.U.R. Weizenecker, Tomographic imaging using the nonlinear response of magnetic particles. *Nature*, 2005.
- [2] Graeser, M., et al., Human-sized magnetic particle imaging for brain applications. *Nature Communications*, 2019. 10(1): p. 1936.
- [3] Top, C.B., et al., Trajectory analysis for field free line magnetic particle imaging. *Medical Physics*, 2019.
- [4] Goodwill, P.W. and S.M. Conolly, The X-Space Formulation of the Magnetic Particle Imaging Process: 1-D Signal, Resolution, Bandwidth, SNR, SAR, and Magneto stimulation. *IEEE Transactions on Medical Imaging*, 2010: p. 1851–1859.
- [5] Kilic, B., et al., Inverse Radon transform-based reconstruction with an open-sided magnetic particle imaging prototype.